High-Cooperativity Cavity QED with Magnons at Microwave Frequencies

Maxim Goryachev,[1] Warrick G. Farr,[1] Daniel L. Creedon,[1] Yaohui Fan,[1] Mikhail Kostylev,[2] and Michael E. Tobar[1,*]

[1]*ARC Centre of Excellence for Engineered Quantum Systems, School of Physics, University of Western Australia, 35 Stirling Highway, Crawley, Western Australia, 6009, Australia*

[2]*Magnetisation Dynamics and Spintronics Group, School of Physics, University of Western Australia, 35 Stirling Highway, Crawley, Western Australia, 6009, Australia*

(Received 25 July 2014; revised manuscript received 10 October 2014; published 5 November 2014)

Using a submillimeter-sized YIG (yttrium-iron-garnet) sphere mounted in a magnetic-field-focusing cavity, we demonstrate an ultrahigh cooperativity of 10^5 between magnon and photon modes at millikelvin temperatures and microwave frequencies. The cavity is designed to act as a magnetic dipole by using a novel multiple-post approach, effectively focusing the cavity magnetic field within the YIG crystal with a filling factor of 3%. Coupling strength (normal-mode splitting) of 2 GHz (equivalent to 76 cavity linewidths or 0.3 Hz per spin) is achieved for a bright cavity mode that constitutes about 10% of the photon energy and shows that ultrastrong coupling is possible in spin systems at microwave frequencies. With straightforward optimizations we demonstrate that this system has the potential to reach cooperativities of 10^7, corresponding to a normal-mode splitting of 5.2 GHz and a coupling per spin approaching 1 Hz. We also observe a three-mode strong-coupling regime between a dark cavity mode and a magnon-mode doublet pair, where the photon-magnon and magnon-magnon couplings (normal-mode splittings) are 143 and 12.5 MHz, respectively, with a HWHM bandwidth of about 0.5 MHz.

DOI: 10.1103/PhysRevApplied.2.054002

I. INTRODUCTION

The field of quantum information has achieved significant progress in recent decades, and its continued success is driven by a strong focus on quantum technology. Ongoing development of the devices and experimental techniques that utilize the quantum nature of the world to perform storage, transfer, and processing of quantum information is critical to achieving the ambitious goal of workable quantum computation. The mainstream framework used to reach this goal is known as quantum electrodynamics (QED), having roots in the Jaynes-Cummings (JC) model and its variations [1,2]. Under this framework, a high-fidelity technology must be able to exchange information with preserved coherence, i.e., to demonstrate the so-called strong-coupling regime, which is represented by a cooperativity greater than unity. This criteria, which must be met in order to be useful for any quantum application, is characterized by a coupling between two subsystems that is stronger than the mean of the losses in both of them. In the present work, this is the regime in which the photon-magnon coupling is greater than the average of the resonant cavity and resonant-magnon losses.

Achieving operation in a strong-coupling regime is a challenging task, because one usually encounters contradictory requirements for the coupling of a system to its environment. In this work, we push the limits of what is currently possible and achieve extremely high cooperativity at microwave frequencies. Such cooperativities have been achieved previously only in optical systems coupled to the motion of neutral atoms [3]. The unique nature of the system described herein allows the "ultrastrong"-coupling regime to be approached, in which the coupling energy is comparable to that of the subsystem itself [4–7]. This relation between the energy of the coupled and uncoupled system invalidates the use of the usual rotating-wave approximation, and thus leads to a breakdown of the Jaynes-Cummings model. The resulting system is analytically unsolvable and demonstrates complex dynamics that may include frequency renormalization, revival and collapse of coherent oscillations, and chaotic behavior [8,9]. The ultrastrong-coupling regime has been observed only in certain systems at optical frequencies [10–14], in artificially created matter, and with superconducting qubits [5,6]. However, with a specially designed photonic cavity, this regime may also be achieved in a submillimeter-sized spin system at microwave frequencies. Previous work [12] has achieved ultrastrong "light-matter" coupling through electric near-field enhancement using an electric dipole. The present work is the magnetic analogue of this, instead using a magnetic dipole configuration to enhance the field within the sample.

The first step towards a new physical realization of a scheme for manipulating quantum information requires that a proper choice of subsystems be made. While one of the subsystems is typically an electromagnetic cavity, the other must demonstrate quantum behavior, preferably with long coherence times. Examples of the latter subsystem are

*michael.tobar@uwa.edu.au

numerous and range from mechanical oscillators in their quantum ground state to trapped single ions. For the former subsystem, a choice is typically made between a 2D or a 3D electromagnetic cavity. Despite recent progress in 2D planar superconducting structures, the use of 3D structures has gained broad interest in recent years and continues to gain momentum [15,16].

A number of physical realizations have been proposed recently for the "quantum" subsystem that include trapped ions [17], superconducting qubits [18], quantum dots [19], photonic nanostructures [20], ultracold atoms and ensembles [21], and electronic and nuclear spins in solids [22]. In particular, one possible realization of an optical-to-microwave quantum interface [23] is based on spin-doped dielectric crystals such as Fe^{3+} ions in sapphire [24], Er^{3+} in yttrium orthosilicate [25,26], or nitrogen-vacancy (NV) centers in diamond [27]. The use of large-spin ensembles for quantum information processing has been discussed previously by Imamoglu [28], who claims that collective excitations of spin ensembles can be incorporated into hybrid systems with a nonlinear element such as a Josephson junction. This includes the possibility to design new protocols without single-spin confinement [28]. In general, large-spin ensembles are considered to be of great potential importance for application to hybrid quantum systems and quantum information manipulation, with considerable work invested in this area by many groups [22,29–31].

The utilization of spin-doped 3D cavities can lead to operation in the strong-coupling regime, however, the coupling strength always stays limited because an increase in the number of spins usually leads to a broadening of both the spin and cavity resonances causing a trade-off with electromagnetic coupling. This problem may be solved by using dielectrics that exhibit ferromagnetism instead of dilute paramagnetic impurities. Because ferromagnetic materials are perfectly ordered systems, they do not suffer from excess losses due to spin-spin interactions when the spin density is increased. At the same time, ferrite materials have much larger magnetic susceptibilities than paramagnetic systems due to the vastly increased number of spins, thus having the potential for much stronger cavity-spin coupling per unit volume. Furthermore, ferromagnetic magnon resonances could be compared to mechanical modes, another important element of optomechanics-based quantum-hybrid systems [32]. A natural choice for a ferromagnetic system is single-crystal YIG, or yttrium iron garnet [$Y_3Fe_2(FeO_4)_3$] [33], a ferrite material with unique microwave properties. YIG exhibits a record low microwave magnetic-loss parameter, and excellent dielectric properties at microwave frequencies. For this reason, it has been extensively studied at room temperature for various microwave and optical applications. Strong-coupling regimes in YIG nanomagnets have already been predicted [34–36], and although some preliminary attempts have been made to couple superconducting planar cavities [37] and 3D resonators [38,39] to magnon resonances in YIG, the potential of the material has not yet been fully explored. Thus, the combination of a specially designed 3D cavity and a YIG ferromagnet represents a promising path towards the ultrastrong-coupling regime of QED.

Specifically, in the present work we use a submillimeter-sized YIG sphere mounted in a 3D microwave cavity at millikelvin temperatures and approach the ultrastrong-coupling regime between magnon and photon modes in the system. The cavity is designed using a novel, patented [40], multiple-post reentrant cavity concept. This configuration effectively focuses the resonant magnetic field into the submillimeter-sized YIG crystal to achieve extraordinarily large filling factors at microwave frequencies. Such a large magnetic filling factor is possible despite the fact that the smallest resonant frequency of the YIG crystal itself is of the order of 100 GHz. Coupling strength of 2 GHz is achieved for the bright cavity mode, which constitutes about 10% of the photon energy, or nearly 76 cavity linewidths. In addition, a three-mode strong-coupling regime is observed between a dark cavity mode and two magnon modes, where the photon-magnon and magnon-magnon couplings are 143 and 12.5 MHz, respectively. Multiple magnon modes of the YIG sphere are observed with bandwidths approaching 0.5 MHz.

II. CAVITY WITH MAGNETIC FIELD FOCUSING

Because of the peculiar structure of magnon modes in a ferromagnetic material, the optimal shape of a 3D ferromagnetic resonator is a miniature sphere. As such, best commercial-quality YIG crystals typically come in the form of spheres for microwave applications, however, technological limitations place bounds on the maximum volume of such crystals. Single-crystal spherical YIG resonators can typically be manufactured with a diameter in the range of 200–1000 μm. These dimensions make the corresponding resonant frequencies of electromagnetic modes in the sphere above 100 GHz. Thus, it is impossible to utilize the sphere itself as a photon cavity in the X and K_u microwave-frequency bands, and one must instead rely on coupling of the ferromagnetic resonance in the sphere to some external resonator, for example, a 3D microwave cavity. For a traditional rectangular microwave cavity, the half wavelength of the lowest order standing wave resonance is equal to the cavity size. In the X and K_u bands, the half wavelength is much greater than the diameter of the sphere, strongly reducing the coupling of the sphere to the cavity. In the present work we use a novel design of reentrant cavity with two posts to increase the filling factor of the cavity volume with the YIG material, and thus enhance the coupling. In comparison, recent work which couples standard cavities to similar YIG spheres obtained

significantly lower filling factors, cooperativity, and coupling per spin [38,39].

A reentrant cavity [41–43] is a closed (typically cylindrical) 3D microwave resonator built around a central post with an extremely small gap between one of the cavity walls and the post tip. Such a cavity is characterized by spatial separation of the electric and magnetic components of the cavity field. Whereas most of the electric field is concentrated in the gap, all of the magnetic field is distributed around the post, with a fast radial decay in amplitude. In fact, a reentrant cavity can be considered the 3D realization of a lumped LC circuit and thus can operate in a subwavelength regime.

Microwave reentrant cavities as described have a well-confined electrical field, but the magnetic field is distributed over quite some volume, which is significantly larger than that of a typical YIG sphere. Thus, it is a necessity to focus this field into a relatively small region of the cavity, a problem that is solved by employing a double-post structure [see Fig. 1(a)] which is the simplest case of a 3D reentrant cavity lattice [44]. Such multiple-post reentrant cavities are the subject of a patent [40]. In fact, each post acts as a separate microwave resonator since each has its own equivalent inductance and capacitance. As a result, the overall system has two modes: a dark mode and a bright mode. An electrical analogue of this approach has been used previously to enhance electrical coupling between surface plasmons and molecular excitons [12].

For the dark mode (Fig. 1, labeled ↑↑), the current through both posts flows in the same direction, making the $\vec{B}$ field around each post curl in the same direction. As a result, the vectors of the $\vec{B}$ field from the two posts are antiparallel in the space between the posts, effectively canceling the field. Elsewhere, the field vectors are almost coaligned, thus enhancing the field. The result of finite-element modeling of the magnetic-field distribution for such a mode is shown in Fig. 1(b). The model takes into account the presence of a YIG sphere at zero external applied magnetic field. Since all of the electric field is concentrated in the post gaps and no magnetic response is seen at zero field, the presence of the sphere is a small perturbation of the solution. In the case of the bright mode (Fig. 1, labeled ↑↓), the currents through the posts are always opposite, making the $\vec{B}$ field for each post curl in the opposite direction. As a result, the total $\vec{B}$ field is enhanced between the posts and canceled elsewhere. The distribution of magnetic field for the bright mode is shown in Fig. 1(b). The system described is similar to the magnetic field of a current loop. In the plane of the loop, the fields generated by any two opposite loop sections are added in phase within the bounded area of the loop, and out of phase outside the loop area. This strongly enhances the total field inside the loop and effectively cancels it outside. Thus, the cavity presented here can be understood as a two-dimensional current dipole. Note that for both cavity modes the microwave magnetic field lies perfectly in the plane perpendicular to the posts.

This work confirms that the presence of the two posts makes it possible to produce excellent confinement of the magnetic component of the cavity field in the small volume between the posts. This field-focusing effect results in very high spatial overlap between the photon mode of the cavity and the magnon mode of the YIG crystal, and thus the strong coupling between them. The overlap is usually

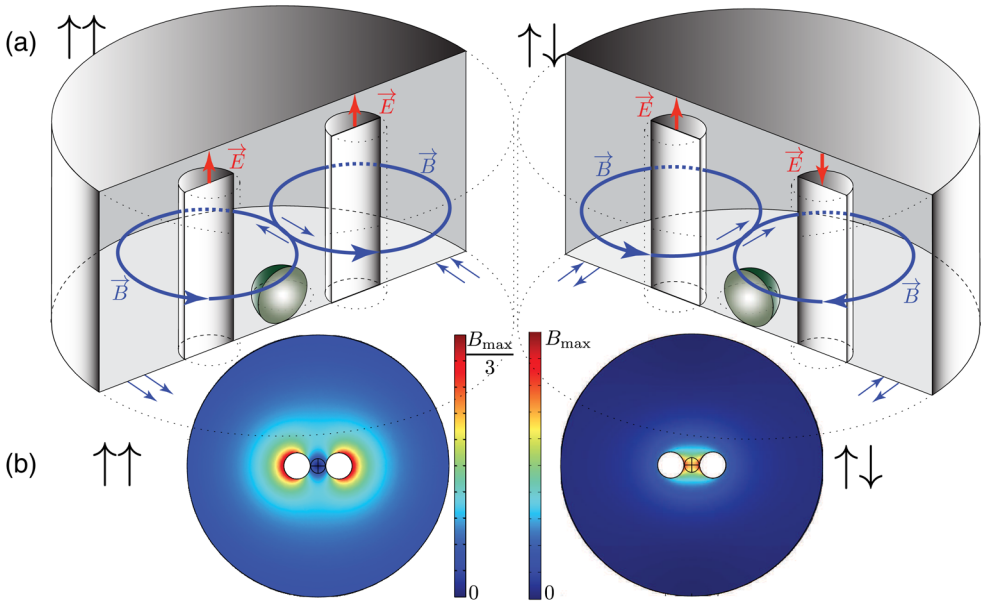

FIG. 1. Two reentrant-type cavities with two resonance posts. Cavity ↑↑ demonstrates operation in the "dark" mode, and cavity ↑↓ demonstrates operation in the "bright" mode. (a) shows a 3D cross-sectional view of the cavities with $\vec{E}$ and $\vec{B}$ field directions, and (b) shows a top view of the field modeling results computed in the equatorial plane of the YIG sphere.

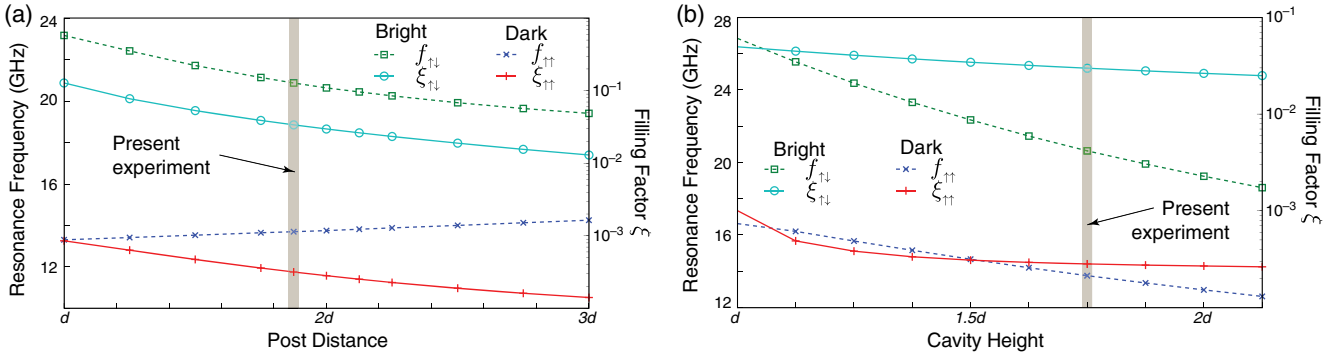

FIG. 2. Cavity-resonance frequencies and YIG-sphere filling factors as a function of (a) the distance between the two posts and (b) the cavity height, for both the dark and bright modes. The distance is given in terms of the sphere diameter d.

characterized by a filling factor ξ that denotes the portion of the total cavity magnetic energy stored in the sphere. Another important experimental parameter is the geometric factor G calculated as follows:

$$G = \omega_0 \mu_0 \frac{\int_V |H|^2 dv}{\int_S |H|^2 ds}, \tag{1}$$

where ω_0 is the angular frequency of a cavity mode, μ_0 is the vacuum permeability, H is the magnetic field in the cavity, and V and S are cavity volume and conducting surface. This parameter relates the electromagnetic cavity Q factor to the surface resistance R_s through the expression $G = QR_s$, assuming that this is the dominant loss mechanism.

Finite-element modeling of the cavity modes allows estimations of the cavity eigenfrequencies, the filling factor ξ, and the geometric factor G. For the actual cavity dimensions (an internal cavity radius of 5 mm, cavity height 1.4 mm, post radius of 0.4 mm, and post gap of 73 μm, distance between the posts 1.5 mm), the predicted resonance frequencies for the dark and bright modes are 13.75 and 20.6 GHz, respectively, which is in good agreement with the experiment. The filling factors for the two modes are 3×10^{-4} and 3×10^{-2}, respectively, a ratio of 2 orders of magnitude. The bright mode is also superior in terms of the geometric factor, 59 Ω versus 51 Ω for the dark mode. Note that the sphere is a small perturbation for the cavity mode when the magnon resonance is tuned away, mainly due to the absence of the electric field between the two posts.

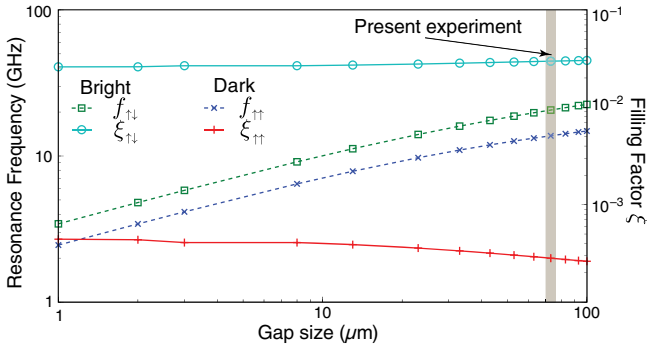

FIG. 3. Cavity-resonance frequencies and the YIG-sphere filling factor as a function the post gap size, for both the dark and bright modes.

Our simulations demonstrate that the filling factor ξ can be further enhanced by optimizing the distance between the posts, and the height of the cavity. In Fig. 2, the cavity-resonance frequencies and filling factors are shown as a function of the corresponding dimensions in units of the sphere diameter $d = 0.8$ mm. A decrease in post spacing to the diameter of the YIG sphere results in a filling-factor increase up to 0.12, whereas reducing the cavity height to the smallest possible value results in a filling factor of 0.05. Applying both optimizations together would result in a filling factor of 0.2, potentially an order of magnitude larger than the present work. Altering these parameters, however, results in an increase of the cavity eigenfrequencies. This drawback can be overcome by adjusting the size of the post gap, to which the cavity-resonance frequency is extremely sensitive (Fig. 3) but the filling factor ξ is completely insensitive. Reducing the gap size leads not only to a decrease in the cavity eigenfrequency, but also to an increase of the geometric factor. Two other major parameters, namely the post radius and the cavity diameter do not significantly change the value of the filling factor, although they can also be used to manipulate the resonant frequency.

III. PHYSICAL REALIZATION

The current dipole cavity is fabricated from oxygen-free-high-conductivity (OFHC) copper with the dimensions corresponding to that used for simulation in the previous section. After insertion of the YIG sphere between the posts, the cavity is cooled to about 25 mK by means of a dilution refrigerator (DR) with a cooling power of about 500 μW at 100 mK. The cavity is attached to a OFHC copper rod bolted to the mixing chamber stage of the DR that places it at the field center of a 7 T superconducting

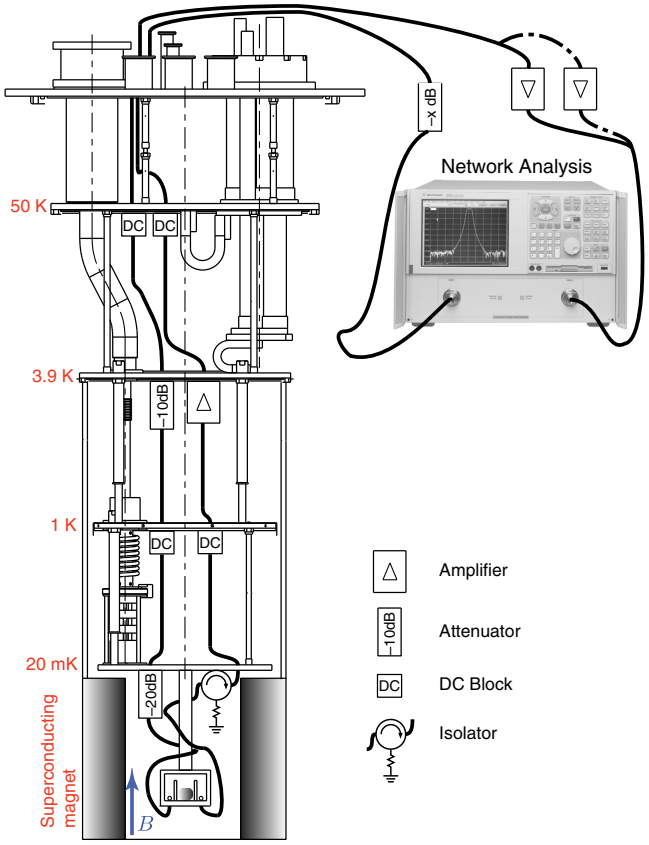

FIG. 4. Schematic of the experiment. For clarity, not all antiradiation shields are shown.

magnet. The magnet is attached to the 4 K stage of the DR, with the cavity mounted within a radiation shield of approximately 100 mK that sits within the bore of the magnet.

A commercially available YIG sphere with a diameter $d = 0.8$ mm attached to a standard beryllium-oxide cylindrical post is used for the experiment. The nominal magnetic losses specified by the manufacturer are 0.2 Oe at room temperature. A cylindrical hole is made centrally in the bottom of the cavity in order to hold the sphere by its beryllium-oxide mounting rod in between the posts. The optimum crystallographic axis for thermal compensation of the sphere is oriented along the posts. Since no thermal stability characterization of the magnon resonance is made in this study, the orientation of the sphere is not important for the present work.

The cavity modes are exited by a loop probe constructed from flexible subminiature version A cable launchers, and measurements are performed through a second loop probe. The incident signals are attenuated by a series of cold attenuators at 3.9 K (−10 dB) and at 20 mK (−20 dB) before reaching the cavity. The power incident on the cavity is set at −90 dBm, while the coupling on both ports does not exceed 0.01 (corresponding to less than 15 photons in the cavity). The transmitted signal is then amplified by a cryogenic low-noise amplifier (Low Noise Factory, 6–20 GHz, 20 dB gain) bolted to the 3.9 K stage. The cryogenic amplifier and the cavity are separated by an isolator situated at the 20 mK stage to prevent backaction noise from the higher-temperature stage. The isolator is shielded from the field of the superconducting magnet. Additional room-temperature amplification is performed via one of two low-noise amplifiers (6–18 GHz and 18–40 GHz), dependent on the frequency band under study. Additional dc blocks are used at various stages of the system in order to suppress spurious low-frequency signals. Both the network analyzer and the superconducting magnet are computer controlled for automatic operation. Figure 4 shows a schematic of the experimental setup.

Note that the superconducting magnet and the cavity are separated by an additional antiradiation shield attached to the 100 mK stage (see Fig. 4). The cavity is firmly connected to the 20 mK stage via a thick oxygen-free high-conductivity copper rod. The cavity is placed at the center of the superconducting magnet where sufficient uniformity of the dc magnetic field is achieved.

IV. EXPERIMENTAL OBSERVATIONS

The cavity is placed under an applied external dc magnetic field swept from 0 to 0.9 T, and its transmission response is recorded using a vector network analyzer. The maximum driving efficiency of magnon modes by a microwave field is achieved when the field is perpendicular to the static magnetic bias field [45]. Accordingly, since the microwave magnetic-field vector is in the plane normal to the posts, the dc magnetic field is oriented parallel to the cavity posts.

Figure 5 demonstrates the microwave response of the cavity with a YIG sphere located between the posts. The response is shown as a function of external magnetic field applied parallel to the posts, with darker color corresponding to higher transmission. The upper-right section of the density plot has a different signal-to-noise ratio than the rest of the data due to the utilization of a different (higher-frequency bandwidth) room-temperature amplifier in that region. The two horizontal lines of higher transmission labeled as $f_{\uparrow\uparrow} = 13.9$ GHz and $f_{\uparrow\downarrow} = 20.9$ GHz correspond to the dark and bright cavity modes, respectively. The line of higher transmission that grows almost linearly with the magnetic field represents the magnon mode of uniform precession in the YIG sphere. In addition to the mode labeled M_1, there are a number of other modes, so-called magnetostatic modes of the ferromagnetic sphere [46,47] visible only in the close vicinity of the cavity resonances. The most prominent of these are labeled M_2 and M_3, and are clearly seen in the inset of the density plot in Fig. 5. A darker region inside the upper interaction is due to line resonances that are removed elsewhere with image postprocessing.

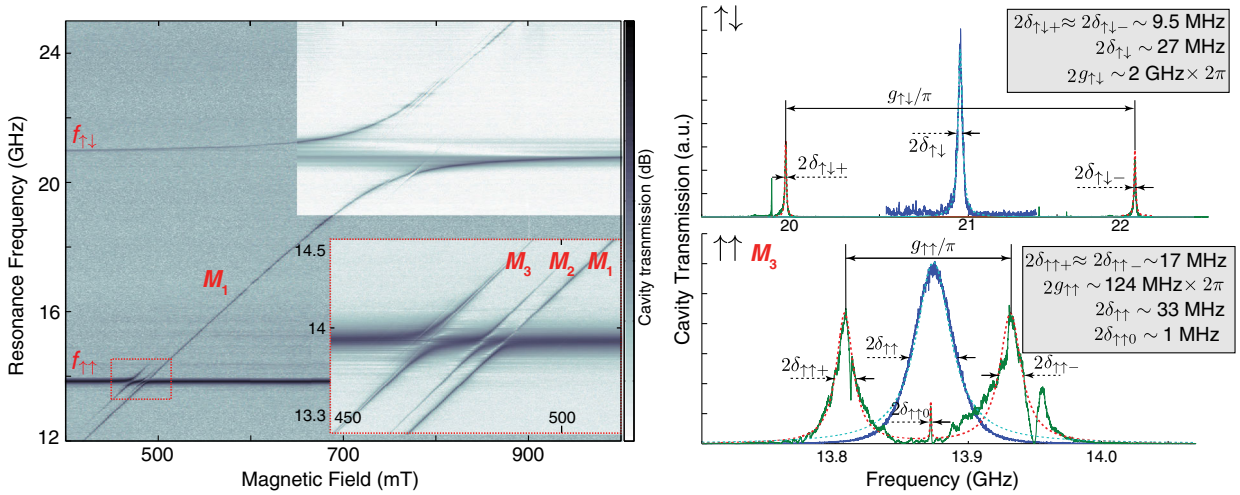

FIG. 5. Transmission through the cavity as a function of frequency and applied dc magnetic field. The inset demonstrates the region of interaction between the dark mode and the magnon resonance. The plot labeled $\uparrow\downarrow$ shows the frequency response of the interaction between the $f_{\uparrow\downarrow}$ cavity mode and the magnon mode M_1 at $B = 0.743$ T, and the bare cavity mode outside resonance. The plot labeled $\uparrow\uparrow$ shows the interaction between $f_{\uparrow\uparrow}$ and the magnon mode M_2 at $B = 0.471$ T, as well as the bare cavity mode outside the resonance. Dashed curves represent Lorentzian fits to the data.

The density plot reveals the existence of several avoided crossings between the magnon modes of the sphere and the two cavity modes. The strongest interaction is observed between the bright cavity resonance and the uniform magnon mode. The corresponding strong-coupling regime achieved at $B = 0.743$ T is demonstrated in the subfigure labeled $\uparrow\downarrow$. This plot displays a central peak representing the bare cavity resonance outside the interaction, with linewidth $2\delta_{\uparrow\downarrow}$ (given in units of Hz), and the splitting between the two peaks in the strong-coupling regime (with linewidths $2\delta_{\uparrow\downarrow+}$ and $2\delta_{\uparrow\downarrow-}$). The condition on the strong coupling is $\frac{g_{\uparrow\downarrow}}{\pi} \gg \delta_{\uparrow\downarrow+} + \delta_{\uparrow\downarrow-}$ and is thus satisfied. The strength of the coupling $g_{\uparrow\downarrow}/\pi$ is approximately 2 GHz, which is 10% of the corresponding resonance frequency $f_{\uparrow\downarrow}$, qualifying it as ultrastrong coupling as discussed in the introduction.

For the dark resonance, the strongest interaction is achieved for the magnon mode M_3 at $B = 0.471$ T and is demonstrated in the subfigure labeled $\uparrow\uparrow$. The field of dynamic magnetization for the M_1 magnon mode is perfectly uniform over the volume of the sphere, but the microwave magnetic field of the dark cavity mode is perfectly antisymmetric with respect to the middle of the distance between the cavity posts. Thus, the M_1 mode does not interact with the dark cavity mode due to the resonant magnetic rf field reversing direction within the sphere, which causes first-order cancellation of the coupling. The strong coupling to the M_3 mode suggests it has two variations of the magnon phase in the azimuthal direction [48]. Thus, it is clear from these results that one must take into account the mode shapes of both the photonic and magnon resonances inside the sphere to properly calculate the coupling for a general photon-magnon-mode interaction.

Various magnon modes of the sphere can be observed at the lower-frequency cavity resonance as depicted in Fig. 6(a). The figure also presents theoretical predictions made based on the existing theory of magnon modes in ferrimagnetic spheroids [46] with a fitted value of saturation magnetization $M = 0.255$ T for various combinations of wave numbers (n, m). Here, for simplicity, we employ a simplified two-index notation dropping the third number referring to the number of the solution [46]. This estimation of the saturation magnetization at 20 mK is in good agreement with previous measurements [49] where it is demonstrated that M grows from 0.175 T at 300 K to 0.244 T at 4 K. Visualizations of magnon modes in a sphere have been computed in the past [48]. The only parameter of the model M is fitted in such a way that the observed mode structure matches the predicted one. Other theoretically predicted modes have frequencies above the analyzed frequency range and cannot be coupled to due to mode symmetries.

The strong-coupling regime between the dark cavity mode and the M_3 magnon resonance is achieved at $B = 0.471$ T, shown in Fig. 6(b). This plot displays a central peak representing the bare cavity resonance $f_{\uparrow\uparrow}$ outside the interaction, having linewidth $2\delta_{\uparrow\uparrow}$, as well as the splitting between the two peaks in the strong-coupling regime (linewidths $2\delta_{\uparrow\downarrow+}$, $2\delta_{\uparrow\downarrow-}$, and $2\delta_{\uparrow\downarrow 0}$). Unlike the case of the magnon mode M_1, which interacts according to a two-mode model with the bright mode, this interaction can be successfully modeled only by using a three-mode model, one of which is the dark cavity mode, and the other two of which are a magnon-mode doublet with the degeneracy lifted.

The origin of the double magnon mode in a spherical geometry has certain similarities with the existence of

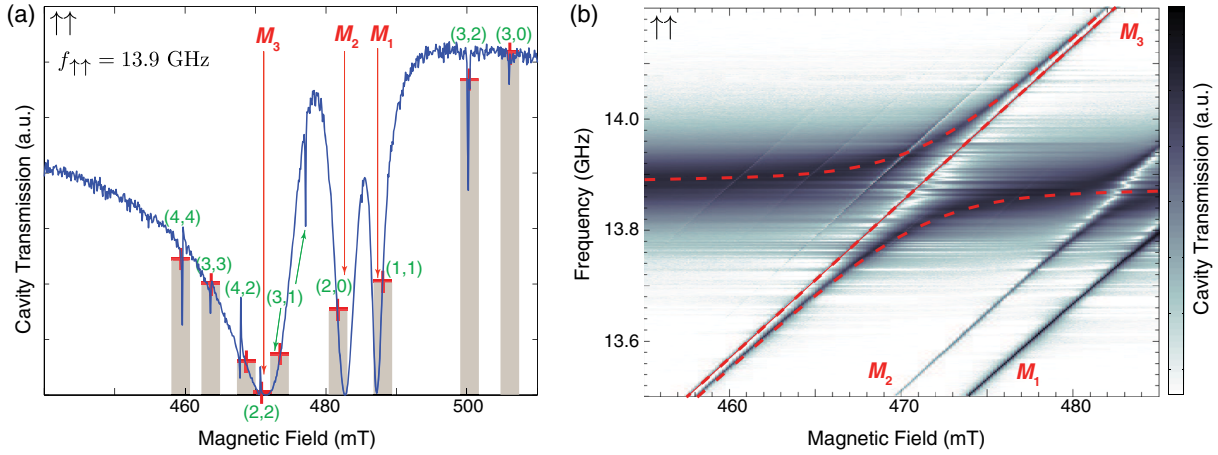

FIG. 6. (a) Magnon modes observed near the dark cavity mode ↑↑ at $f_{\uparrow\uparrow} = 13.9$ GHz. Red crosses and shaded areas are theoretical predictions for magnon modes of order (n, m) [46]; (b) interaction between the magnon doublet M_3 and the dark cavity mode. Avoided crossings between photon and magnon modes are observed as transmission dips. The dashed curves show the three-mode interaction model fit.

whispering-gallery-mode (WGM) doublets that are extensively observed in spherical, toroidal, and cylindrical resonators. The latter phenomenon is related to the existence of counterpropagating photonic modes with the same wave number whose degeneracy is lifted by the existence of backscattering elements. In the present experiment, a doublet of magnon resonances (magnetic in nature) exists where one is strongly coupled to a single photonic cavity resonance, and the second remains unaffected by the interaction. This is opposite to the case in which WGMs interact with paramagnetic impurities in high-Q resonators, where the doublet is instead photonic in nature and interacts with a single (para)magnetic resonance. In this case, one resonance of the WGM doublet couples strongly to the electron spin resonance, and the other does not [50–52].

The magnon linewidths can be estimated by direct measurements of the cavity transmission far from cavity-magnon interactions. The linewidths of the uncoupled uniform magnon mode M_1 and mode M_2 are measured to be approximately $2\delta_{M1} = 1.1$ MHz and $2\delta_{M2} = 760$ kHz. The doublet magnon mode M_3 exhibits linewidths of 1.2 MHz and 490 kHz for the interacting and noninteracting resonances, respectively. The sub-MHz linewidth of the YIG magnon resonances place it in front of the many other well-studied dilute spin systems such as Er^{3+} and Eu^{3+} and in Y_2SiO_5 (~7–24 MHz) [26], Cr^{2+} and Fe^{3+} in sapphire (9 and 27 MHz) [24], Er^{3+} in $YAlO_3$ (~15–33 MHz) [53], etc., but behind such systems as nitrogen vacancy centers in diamond [22]. Traditionally, the loss rate in resonant spin systems is expressed as an applied-field-resolved resonance linewidth (half width at half maximum). For the sphere in this work, the resonance linewidth is 0.2 Oersted, as specified by the manufacturer and is confirmed by the present measurements. By multiplying this value by the gyromagnetic coefficient extracted from our experimental data, one obtains the frequency-resolved resonance linewidth slightly below 1 MHz, which is consistent with our results. It should be mentioned that the single-crystal YIG is the material with the lowest known ferromagnetic loss at microwave frequencies, far exceeding other ferri- or ferromagnetic materials. Furthermore, the shape of a (small) sphere ensures the highest possible symmetry for the collective dynamics of strongly exchange-coupled spins. This further decreases magnetic losses by prohibiting several processes leading to resonance-linewidth broadening. These processes include a number of magnon-magnon scattering processes, as well as losses due to the excitation of higher-order resonances and traveling spin waves. Higher-order magnon modes observed in the experiment are absent at room temperature, but their appearance at cryogenic temperatures may be explained by mechanical stress induced in the sphere during the cooldown procedure, which slightly breaks the symmetry of the spin dynamics.

The cavity linewidths are 33 and 27 MHz corresponding to Q factors of 520 and 714, respectively, for the dark and bright modes. Using these results and the simulated values of the geometric factor G, we estimate the effective surface resistance of the cavity to be 76 mΩ. It should be noted that the cavity is fabricated from the OFHC copper and is not optimized in terms of loss. In particular, the inner surfaces of the cavity have not been polished and are oxidized. The surface resistance of ultrapure polished copper at millikelvin temperatures is about 9 mΩ, which could result in a considerable reduction of cavity bandwidths. Because of comparatively high cavity losses, the system demonstrates no nonlinear effects around the working incident power. The number of cavity photons is estimated to be less than 15 on resonance from the known incident power to the cavity, coupling, and Q factor [54,55].

V. PHOTON-MAGNON INTERACTION

The interaction between the bright cavity mode and the uniform magnon mode of the sphere can be described by the Hamiltonian of a harmonic oscillators (HO) coupled to an ensemble of spins [34–36]:

$$H_{\uparrow\downarrow M_1} = \hbar\omega_{\uparrow\downarrow} a^\dagger a + \frac{g\mu_B}{2} B S_z - \hbar g_{\uparrow\downarrow}(S_+ a + a^\dagger S_-) + H_{\text{non-JC}}(aS^-, a^\dagger S^+), \quad (2)$$

where g is the electron g factor, μ_B is the Bohr magneton, B is the applied dc magnetic field, $a^\dagger$ and a are the creation and annihilation operators for the bright cavity mode, $\omega_{\uparrow\downarrow}$ is the corresponding angular frequency, $g_{\uparrow\downarrow}$ are coupling constants of the modes to the spins, and S^z (S^+ and S^-) are the collective spin operators. The latter are operators whose eigenstates $|l, m\rangle$ are similar to that in the Dicke model [56], i.e., $S_\pm|l, m\rangle = \sqrt{(l \mp m)(l \pm m + 1)}|l, m \pm 1\rangle$. Note that the final term of the Hamiltonian is the typically oscillating "counterrotating" term, and is always neglected when using the rotating-wave approximation.

The first term of the Hamiltonian represents a HO corresponding to the bright cavity mode. The second term represent a collective spin with the frequency $\omega = \frac{g\mu_B}{\hbar} B$, and the last term determines the coupling between the cavity and the uniform magnon mode. From Eq. (2) it follows that one can use the standard model of two interacting HOs to fit the experimental data. This fit gives the coupling constant $g_{\uparrow\downarrow}/\pi = 2.05$ GHz or $2g_{\uparrow\downarrow}/\omega_{\uparrow\downarrow} \approx 10\%$.

As discussed previously, the interaction between the dark cavity mode and magnon mode M_3 is essentially a three-mode interaction. This follows from the fact that the observed interaction cannot be approximated by the two-mode model, and is also confirmed by the existence of the degeneracy in the M_3 mode. The corresponding fit of the three-mode model interaction is shown in Fig. 6(b). This density plot demonstrates a central magnon line not interacting with an avoided crossing which it passes. As a result, one observes simultaneously three resonant peaks at a cross-section which passes the center of the avoided crossing. Since the upper and lower parts of the avoided crossing do not converge to the same asymptote, the system cannot be fit by the two-oscillator model. The difference between the upper and lower asymptotes defines the coupling between the two almost degenerate magnon modes. Such a three-mode model has been previously utilized for high-Q whispering-gallery-mode systems to fit interactions between two center-propagating near-degenerate photon modes and a spin ensemble [51,52]. Thus, the three-mode system appears as follows:

$$H_{\uparrow\uparrow M_3} = \hbar\omega_{\uparrow\uparrow} b^\dagger b + \left(\frac{g\mu_B}{2} B + \omega_R\right) c_R^\dagger c_R + \left(\frac{g\mu_B}{2} B + \omega_L\right) c_L^\dagger c_L + \hbar g_{RL}(c_R c_L^\dagger + c_R^\dagger c_L) - \hbar g_{\uparrow\uparrow}(c_R^\dagger a + a^\dagger c_R), \quad (3)$$

where ω_R and ω_L characterize the two doublet frequencies of the M_3 magnon mode, with creation (annihilation) operators $c_R^\dagger$ (c_R) and $c_L^\dagger$ (c_L) coupled via a backscattering mechanism with strength g_{RL}. As follows from this fit [dashed curves in Fig. 6(b)], only one of the counter-propagating modes of the doublet is coupled to the photon cavity resonance, with strength $g_{\uparrow\uparrow}$. As shown in Fig. 6, M_3 is the (2,2)-sphere magnon mode, which implies the existence of a spatially orthogonal degenerate doublet. Figure 7 captures the origin of the difference in couplings to this doublet: whereas one realization of the (2,2) mode maximizes overlapping between the cavity rf magnetic field $\vec{B}$ and sphere rf magnetization $\vec{m}$, the other minimizes this quantity. The fit to the three-mode HO model given in Eq. (3) gives two coupling constants $g_{\uparrow\uparrow}/\pi \approx 143$ MHz and $g_{RL}/\pi \approx 12.5$ MHz. ince $g_{\uparrow\uparrow}/\pi \gg \frac{1}{2}(\delta_{\uparrow\uparrow} + \delta_{M_3})$, this interaction also satisfies the condition of the strong-coupling regime $\frac{g_{\uparrow\uparrow}}{\pi} \gg \delta_{\uparrow\uparrow+} + \delta_{\uparrow\uparrow-}$ as demonstrated in the $\uparrow\uparrow$ plot of Fig. 5. The corresponding spin cooperativities $\frac{g_{\uparrow x}^2}{(\pi)^2 \delta_M \delta_{\uparrow x}}$ for the dark and bright modes are 1.6×10^3 and 1.3×10^5, respectively.

The predicted filling factors may be related to actual measurement of the magnon-photon coupling as $g_{\uparrow x} = \omega_{\uparrow x}\sqrt{\chi \xi_{\uparrow x}}$, where χ is the effective susceptibility of the YIG, $\omega_{\uparrow x}$ is either $\omega_{\uparrow\downarrow}$ or $\omega_{\uparrow\uparrow}$, and $\xi_{\uparrow x}$ is the corresponding calculated filling factor. The ratio between magnon-photon couplings is thus given as follows:

$$\frac{g_{\uparrow\downarrow}}{g_{\uparrow\uparrow}} = \frac{\omega_{\uparrow\downarrow}}{\omega_{\uparrow\uparrow}} \sqrt{\frac{\xi_{\uparrow\downarrow}}{\xi_{\uparrow\uparrow}}}. \quad (4)$$

The left-hand side of this expression estimated from the actual experiment is 14.5, whereas the right-hand found from the modeling is 15.0, demonstrating good agreement

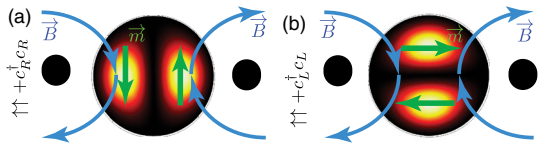

FIG. 7. Origins of the different couplings of the dark cavity mode to two orthogonal realizations [$c_R^\dagger c_R$ (a) and $c_L^\dagger c_L$ (b) in Eq. (3)] of the M_3 mode which is (2,2) magnon-sphere mode. The plot shows the top cavity view with two black circles denoting the post orientation with respect to the sphere.

between modeling and experiment. Further optimization of the cavity dimensions, as has already been discussed, should result in an increase of the coupling strength to 5.2 GHz, representing about 24% of the total cavity energy. Such an optimized system is characterized by a spin cooperativity of 9.1×10^5, an increase over the current cooperativity by a factor of 7 assuming that the cavity parameters remain the same.

Assuming spin density in YIG to be 2.1×10^{22} cm^{-3} [38], the coupling per spin achieved in this work can be estimated to be 0.3 Hz. This value is almost an order of magnitude larger than previously achieved 0.038 Hz in a microwave cavity [38] and considerably larger than for a millimeter-wave cavity 0.067 Hz [39]. As for the latter work, similar results in terms of coupling strength have been achieved by scaling down the size of the cavity leading to an increase of resonant frequencies. However, a shift to the millimeter-wave frequency range leads to additional complications related to higher loss and the requirement for larger magnetic fields.

VI. PREDICTIONS FOR THE OPTIMIZED CAVITY

The results obtained in this work are preliminary and there is a great potential for further improvement. In particular, in order to decrease the cavity frequency such that magnon-photon interactions can occur in the low-gigahertz range and at a low dc magnetic field, the post gap size can simply be reduced. Gap sizes on the order of micrometers to tens of micrometers are easily obtained, which will allow the tuning of such cavities to a few gigahertz. With more advanced manufacturing technology, we anticipate that reduction of the gap size could be even further reduced to the nanoscale. An alternative approach to reduce the cavity frequency is to utilize a more complicated post structure [40,44] or to fill the cavity gap with high-permittivity dielectric which increases the equivalent capacitance. Here, we predict the system response only when the cavity parameters are optimized using realistic values, easily obtainable in the next design iteration. As discussed in the paper, Fig. 8 shows the system response with a predicted photon-magnon coupling of 5.2 GHz for the bright photonic mode. Here, the asymmetry of the interaction is enhanced, which is a property of the ultra-strong-coupling regime. The dark mode exhibits similar enhancement, but the coupling strength always stays an order of magnitude lower.

In addition to the enhancement of the coupling, further optimization will lead to an increase in the geometric factor by up to a factor of 2. This, together with applying standard surface polishing and surface treatment techniques to improve the surface resistance of the cavity, should see at least a 12-fold reduction of the cavity linewidth. These improvements potentially lead to a very large enhancement of the cooperativity of the photon-magnon coupling in this type of a microwave cavity. From these estimations, a value of 1.1×10^7 should be possible, which is almost a factor of 100 times better than the results reported in this work. This would correspond to a coupling per spin as high as 0.77 Hz.

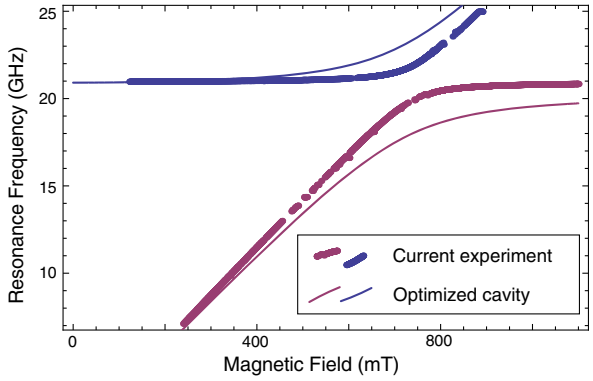

FIG. 8. Predictions of the optimized system response with the cavity tuned to the resonant frequency observed in the experiment.

In conclusion, we have demonstrated strong coupling of 2 GHz and high cooperativity of 10^5 between a photonic mode of a field-focusing double-post microwave reentrant cavity and magnon resonances of a submillimeter-size YIG sphere. The novel cavity design allowed the magnetic filling factor within the small spherical sample to be much larger than possible using standard cavity techniques. The same cavity allowed much lower cavity-resonant frequencies to be achieved than the resonant frequencies of the sample itself. The unique properties of the cavity allow us to better utilize high spin density of the YIG crystal for cavity QED experiments.

ACKNOWLEDGMENTS

This work was supported by the Australian Research Council Grants No. CE110001013, No. FL0992016, and No. DP110103980.

[1] E. T. Jaynes and F. W. Cummings, Comparison of quantum and semiclassical radiation theories with application to the beam maser, Proc. IEEE **51**, 89 (1963).

[2] Michael Tavis and Frederick W. Cummings, Exact solution for an n-molecule-radiation-field Hamiltonian, Phys. Rev. **170**, 379 (1968).

[3] Subhadeep Gupta, Kevin L. Moore, Kater W. Murch, and Dan M. Stamper-Kurn, Cavity nonlinear optics at low photon numbers from collective atomic motion, Phys. Rev. Lett. **99**, 213601 (2007).

[4] Cristiano Ciuti and Iacopo Carusotto, Input-output theory of cavities in the ultrastrong-coupling regime: The case of time-independent cavity parameters, Phys. Rev. A **74**, 033811 (2006).

[5] M. H. Devoret, Steven Girvin, and Robert Schoelkopf, Circuit-QED: How strong can the coupling between a

Josephson junction atom and a transmission line resonator be?, Ann. Phys. (Berlin) **16**, 767 (2007).

[6] T. Niemczyk, F. Deppe, H. Huebl, E. P. Menzel, F. Hocke, M. J. Schwarz, J. J. Garcia-Ripoll, D. Zueco, T. Hummer, E. Solano, A. Marx, and R. Gross, Circuit quantum electrodynamics in the ultrastrong-coupling regime, Nat. Phys. **6**, 772 (2010).

[7] Jonathan Plumridge, Edmund Clarke, Ray Murray, and Chris Phillips, Ultra-strong-coupling effects with quantum metamaterials, Solid State Commun. **146**, 406 (2008).

[8] S. Agarwal, S. M. Hashemi Rafsanjani, and J. H. Eberly, Tavis-Cummings model beyond the rotating wave approximation: Quasidegenerate qubits, Phys. Rev. A **85**, 043815 (2012).

[9] E. K. Irish, J. Gea-Banacloche, I. Martin, and K. C. Schwab, Dynamics of a two-level system strongly coupled to a high-frequency quantum oscillator, Phys. Rev. B **72**, 195410 (2005).

[10] C. Maissen, G. Scalari, D. Turčinková, D. Hagenmüller, S. De Liberato, C. Ciuti, C. Reichl, D. Schuh, W. Wegscheider, M. Beck, and J. Faist, Ultrastrong coupling of the cyclotron transition of a 2D electron gas to a THz metamaterial, Science **335**, 1323 (2012).

[11] Stéphane Kéna-Cohen, Stefan A. Maier, and Donal D. C. Bradley, Ultrastrongly coupled exciton–polaritons in metal-clad organic semiconductor microcavities, Adv. Opt. Mater. **1**, 827 (2013).

[12] Andrea E. Schlather, Nicolas Large, Alexander S. Urban, Peter Nordlander, and Naomi J. Halas, Near-field mediated plexcitonic coupling and giant Rabi splitting in individual metallic dimers, Nano Lett. **13**, 3281 (2013).

[13] T. Schwartz, J. A. Hutchison, C. Genet, and T. W. Ebbesen, Reversible switching of ultrastrong light-molecule coupling, Phys. Rev. Lett. **106**, 196405 (2011).

[14] Y. Todorov, A. M. Andrews, R. Colombelli, S. De Liberato, C. Ciuti, P. Klang, G. Strasser, and C. Sirtori, Ultrastrong light-matter coupling regime with polariton dots, Phys. Rev. Lett. **105**, 196402 (2010).

[15] Hanhee Paik, D. I. Schuster, Lev S. Bishop, G. Kirchmair, G. Catelani, A. P. Sears, B. R. Johnson, M. J. Reagor, L. Frunzio, L. I. Glazman, S. M. Girvin, M. H. Devoret, and R. J. Schoelkopf, Observation of high coherence in Josephson junction qubits measured in a three-dimensional circuit QED architecture, Phys. Rev. Lett. **107**, 240501 (2011).

[16] Chad Rigetti, Jay M. Gambetta, Stefano Poletto, B. L. T. Plourde, Jerry M. Chow, A. D. Córcoles, John A. Smolin, Seth T. Merkel, J. R. Rozen, George A. Keefe, Mary B. Rothwell, Mark B. Ketchen, and M. Steffen, Superconducting qubit in a waveguide cavity with a coherence time approaching 0.1 ms, Phys. Rev. B **86**, 100506 (2012).

[17] M. Gessner, M. Ramm, T. Pruttivarasin, A. Buchleitner, H-P. Breuer, and H. Haffner, Local detection of quantum correlations with a single trapped ion, Nat. Phys. **10**, 105 (2014).

[18] A. Wallraff, D. I. Schuster, A. Blais, L. Frunzio, R. S. Huang, J. Majer, S. Kumar, S. M. Girvin, and R. J. Schoelkopf, Strong coupling of a single photon to a superconducting qubit using circuit quantum electrodynamics, Nature (London) **431**, 162 (2004).

[19] J. P. Reithmaier, G. Sek, A. Loffler, C. Hofmann, S. Kuhn, S. Reitzenstein, L. V. Keldysh, V. D. Kulakovskii, T. L. Reinecke, and A. Forchel, Strong coupling in a single quantum dot-semiconductor microcavity system, Nature (London) **432**, 197 (2004).

[20] Yoshiya Sato, Yoshinori Tanaka, Jeremy Upham, Yasushi Takahashi, Takashi Asano, and Susumu Noda, Strong coupling between distant photonic nanocavities and its dynamic control, Nat. Photonics **6**, 56 (2012).

[21] K. Henschel, J. Majer, J. Schmiedmayer, and H. Ritsch, QED with an ultracold ensemble on a chip: Prospects for strong magnetic coupling at finite temperatures, Phys. Rev. A **82**, 033810 (2010).

[22] R. Amsüss, Ch. Koller, T. Nöbauer, S. Putz, S. Rotter, K. Sandner, S. Schneider, M. Schramböck, G. Steinhauser, H. Ritsch, J. Schmiedmayer, and J. Majer, Cavity QED with magnetically coupled collective spin states, Phys. Rev. Lett. **107**, 060502 (2011).

[23] Sh. Barzanjeh, M. Abdi, G. J. Milburn, P. Tombesi, and D. Vitali, Reversible optical-to-microwave quantum interface, Phys. Rev. Lett. **109**, 130503 (2012).

[24] Warrick G. Farr, Daniel L. Creedon, Maxim Goryachev, Karim Benmessai, and Michael E. Tobar, Ultrasensitive microwave spectroscopy of paramagnetic impurities in sapphire crystals at millikelvin temperatures, Phys. Rev. B **88**, 224426 (2013).

[25] P. Bushev, A. K. Feofanov, H. Rotzinger, I. Protopopov, J. H. Cole, C. M. Wilson, G. Fischer, A. Lukashenko, and A. V. Ustinov, Ultralow-power spectroscopy of a rare-earth spin ensemble using a superconducting resonator, Phys. Rev. B **84**, 060501 (2011).

[26] S. Probst, H. Rotzinger, S. Wünsch, P. Jung, M. Jerger, M. Siegel, A. V. Ustinov, and P. A. Bushev, Anisotropic rare-earth spin ensemble strongly coupled to a superconducting resonator, Phys. Rev. Lett. **110**, 157001 (2013).

[27] Torsten Gaebel, Michael Domhan, Iulian Popa, Christoffer Wittmann, Philipp Neumann, Fedor Jelezko, James R. Rabeau, Nikolas Stavrias, Andrew D. Greentree, Steven Prawer, Jan Meijer, Jason Twamley, Philip R. Hemmer, and Jorg Wrachtrup, Room-temperature coherent coupling of single spins in diamond, Nat. Phys. **2**, 408 (2006).

[28] Atac Imamoğlu, Cavity QED based on collective magnetic dipole coupling: Spin ensembles as hybrid two-level systems, Phys. Rev. Lett. **102**, 083602 (2009).

[29] Y. Kubo, F. R. Ong, P. Bertet, D. Vion, V. Jacques, D. Zheng, A. Dréau, J.-F. Roch, A. Auffeves, F. Jelezko, J. Wrachtrup, M. F. Barthe, P. Bergonzo, and D. Esteve, Strong coupling of a spin ensemble to a superconducting resonator, Phys. Rev. Lett. **105**, 140502 (2010).

[30] Hua Wu, Richard E. George, Janus H. Wesenberg, Klaus Mølmer, David I. Schuster, Robert J. Schoelkopf, Kohei M. Itoh, Arzhang Ardavan, John J. L. Morton, and G. Andrew D. Briggs, Storage of multiple coherent microwave excitations in an electron spin ensemble, Phys. Rev. Lett. **105**, 140503 (2010).

[31] Xiaobo Zhu, Shiro Saito, Alexander Kemp, Kosuke Kakuyanagi, Shin-ichi Karimoto, Hayato Nakano, William J. Munro, Yasuhiro Tokura, Mark S. Everitt, Kae Nemoto, Makoto Kasu, Norikazu Mizuochi, and Kouichi Semba, Coherent coupling of a superconducting flux qubit to an

electron spin ensemble in diamond, Nature (London) **478**, 221 (2011).

[32] *Cavity Optomechanics: Nano- and Micromechanical Resonators Interacting with Light*, edited by Markus Aspelmeyer, Tobias J. Kippenberg, and Florian Marquardt, Quantum Science and Technology Vol. VIII (Springer, New York, 2014).

[33] V. Cherepanov, I. Kolokolov, and V. Lvov, The saga of YIG: Spectra, thermodynamics, interaction and relaxation of magnons in a complex magnons, Phys. Rep. **229**, 81 (1993).

[34] Ö. O. Soykal and M. E. Flatté, Coherent strong-field coupling of a ferromagnetic nanomagnet with a photonic cavity, SPIE Int. Soc. Opt. Eng., **7760**, 77600G (2010).

[35] Ö. O. Soykal and M. E. Flatté, Size dependence of strong coupling between nanomagnets and photonic cavities, Phys. Rev. B **82**, 104413 (2010).

[36] Ö. O. Soykal and M. E. Flatté, Strong field interactions between a nanomagnet and a photonic cavity, Phys. Rev. Lett. **104**, 077202 (2010).

[37] Hans Huebl, Christoph W. Zollitsch, Johannes Lotze, Fredrik Hocke, Moritz Greifenstein, Achim Marx, Rudolf Gross, and Sebastian T. B. Goennenwein, High cooperativity in coupled microwave resonator ferrimagnetic insulator hybrids, Phys. Rev. Lett. **111**, 127003 (2013).

[38] Yutaka Tabuchi, Seiichiro Ishino, Toyofumi Ishikawa, Rekishu Yamazaki, Koji Usami, and Yasunobu Nakamura, Hybridizing ferromagnetic magnons and microwave photons in the quantum limit, Phys. Rev. Lett. **113**, 083603 (2014).

[39] X. Zhang, Ch.-L. Zou, L. Jiang, and H. X. Tang, Strongly coupled magnons and cavity microwave photons, Phys. Rev. Lett. **113**, 156401 (2014).

[40] M. Goryachev and M. E. Tobar, Microwave frequency magnetic field manipulation systems and methods and associated application instruments, apparatus and system, U.S. Patent No. AU2014,903,143 (12 August 2014).

[41] J-M. Le Floch, Y. Fan, M. Aubourg, D. Cros, N. C. Carvalho, Q. Shan, J. Bourhill, E. N. Ivanov, G. Humbert, V. Madrangeas, and M. E. Tobar, Rigorous analysis of highly tunable cylindrical transverse magnetic mode re-entrant cavities, Rev. Sci. Instrum. **84**, 125114 (2013).

[42] K. Fujisawa, General treatment of re-entrant resonant cavities, IRE Trans. Microwave Theory Tech. **6**, 344 (1958).

[43] W. W. Hansen, A type of electrical resonator, J. Appl. Phys. **9**, 654 (1938).

[44] M. Goryachev and M. E. Tobar, The 3D split-ring reentrant cavity lattice: A new metastructure for engineering arrays of coupled microwave harmonic oscillators, arXiv:1408.3228.

[45] A. G. Gurevich, *Ferrites at Microwave Frequencies* (Consultants Bureau, New York, 1963).

[46] P. C. Fletcher and R. O. Bell, Ferrimagnetic resonance modes in sphere, J. Appl. Phys. **30**, 687 (1959).

[47] G. Wiese, Parametric excitation of spherical modes in ferromagnetic spheres by perpendicular and parallel pumping, Z. Phys. B **82**, 453 (1991).

[48] P. Roschmann and H. Dotsch, Properties of magnetostatic modes in spheroids, Phys. Status Solidi (b) **82**, 11 (1977).

[49] Irvin H. Solt, Temperature dependence of YIG magnetization, J. Appl. Phys. **33**, 1189 (1962).

[50] K. Benmessai, M. E. Tobar, N. Bazin, P-Y. Bourgeois, Y. Kersalé, and V. Giordano, Creating traveling waves from standing waves from the gyrotropic paramagnetic properties of Fe^{3+} ions in a high-Q whispering gallery mode sapphire resonator, Phys. Rev. B **79**, 174432 (2009).

[51] Maxim Goryachev, Warrick G. Farr, Daniel L. Creedon, and Michael E. Tobar, Controlling a whispering-gallery-doublet-mode avoided frequency crossing: Strong coupling between photon bosonic and spin degrees of freedom, Phys. Rev. A **89**, 013810 (2014).

[52] Maxim Goryachev, Warrick G. Farr, Daniel L. Creedon, and Michael E. Tobar, Spin-photon interaction in a cavity with time-reversal symmetry breaking, Phys. Rev. B **89**, 224407 (2014).

[53] A. Tkalčec, S. Probst, D. Rieger, H. Rotzinger, S. Wünsch, N. Kukharchyk, A. D. Wieck, M. Siegel, A. V. Ustinov, and P. Bushev, Strong coupling of an Er^{3+}-doped $YAlO_3$ crystal to a superconducting resonator, Phys. Rev. B **90**, 075112 (2014).

[54] Daniel L. Creedon, Yarema Reshitnyk, Warrick Farr, John M. Martinis, Timothy L. Duty, and Michael E. Tobar, High Q-factor sapphire whispering gallery mode microwave resonator at single photon energies and millikelvin temperatures, Appl. Phys. Lett. **98**, 222903 (2011).

[55] John G. Hartnett, Joerg Jaeckel, Rhys G. Povey, and Michael E. Tobar, Resonant regeneration in the sub-quantum regime—A demonstration of fractional quantum interference, Phys. Lett. B **698**, 346 (2011).

[56] R. H. Dicke, Coherence in spontaneous radiation processes, Phys. Rev. **93**, 99 (1954).